



HAL
open science

Energy Modeling of a Lead-Acid Battery within Hybrid Wind/Photovoltaic Systems

Olivier Gergaud, Gaël Robin, Bernard Multon, Hamid Ben Ahmed

► **To cite this version:**

Olivier Gergaud, Gaël Robin, Bernard Multon, Hamid Ben Ahmed. Energy Modeling of a Lead-Acid Battery within Hybrid Wind/Photovoltaic Systems. European Power Electronic Conference 2003, Sep 2003, TOULOUSE, France. 8pp. hal-00674678

HAL Id: hal-00674678

<https://hal.science/hal-00674678>

Submitted on 27 Feb 2012

HAL is a multi-disciplinary open access archive for the deposit and dissemination of scientific research documents, whether they are published or not. The documents may come from teaching and research institutions in France or abroad, or from public or private research centers.

L'archive ouverte pluridisciplinaire **HAL**, est destinée au dépôt et à la diffusion de documents scientifiques de niveau recherche, publiés ou non, émanant des établissements d'enseignement et de recherche français ou étrangers, des laboratoires publics ou privés.

ENERGY MODELING OF A LEAD-ACID BATTERY WITHIN HYBRID WIND / PHOTOVOLTAIC SYSTEMS

O. GERGAUD, G. ROBIN, B. MULTON, H. BEN AHMED
SATIE - Brittany Branch, ENS de Cachan - Ker Lann Campus
35170 BRUZ (France)

Phone: 33 (0)2-99-05-52-64 - Fax: 33 (0)2-99-05-93-28
name@bretagne.ens-cachan.fr
UMR 8029 CNRS

Abstract: *Within the scope of full-scale energy modeling of a hybrid wind / photovoltaic system coupled to the network, our focus herein lies in a battery set-up that makes use of the CIEMAT model. The implementation and energy-based analysis of this model are conducted with emphasis on the continuous estimation of battery capacity. A measurement vs. model results comparison is then performed under actual operating conditions.*

Keywords: *Battery management, Modelling, Renewable energy systems*

I - Introduction

The work performed as part of the current research lies within the scope of the full-scale energy modeling of a reduced-power hybrid wind/photovoltaic production system (20 ASE modules for a 2-kW polycrystalline silicon peak and two 750-W wind turbines), coupled to the network via a continuous bus and connected to an electrochemical storage device (48 V - 15 kWh) (see Figure 1) [GER 01], [GER 02]. A subsystem modeling approach has been derived in order to obtain a series of models accurate enough to account for energy transfers and fast enough to enable optimizing system design and/or control.

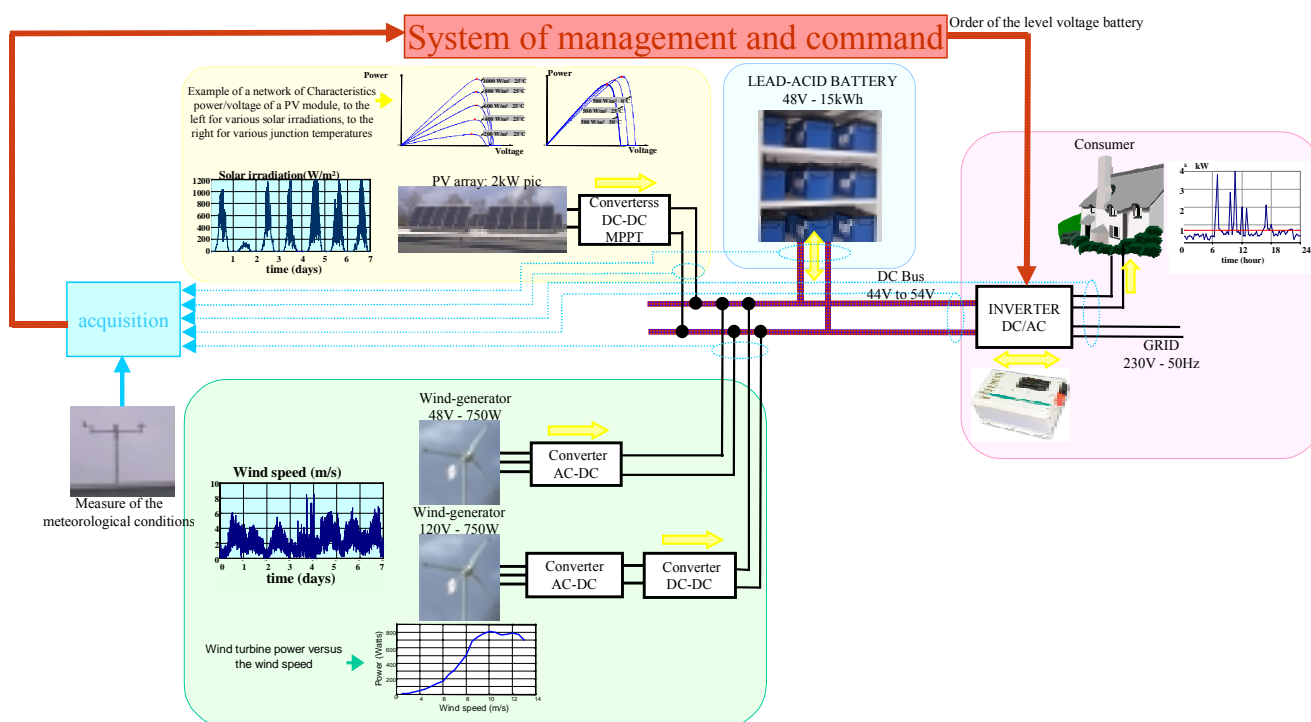


Figure 1: Hybrid wind / photovoltaic production system coupled to the network grid (with energy storage)

The relatively sophisticated nature of the electrochemical accumulators makes it difficult to develop a general model, especially over long-term study periods. The various models identified in the literature, with respect to lead-acid technology, entail a complex implementation due in particular to the high number of parameters to be determined. In order to avoid generating excessive complexity, we have elected to use the CIEMAT model ([COP 93], [DUM 99]), which serves to reproduce correct trends in the actual behavior of electrochemical accumulators while remaining "universal" in its application. As such, no experimental identification of empirical parameters is required when using the other widespread models.

II - The CIEMAT model

This model is based on the electrical diagram presented in Figure 2, according to which the battery is described by just two elements (whose characteristics depend on a set of parameters): a voltage source and the internal resistance.

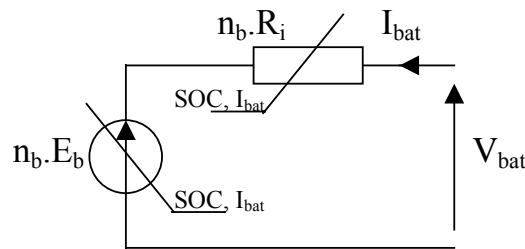


Figure 2: Equivalent electrical diagram of n_b battery elements in series

For the n_b cells in series, the following equation applies:

$$V_{bat} = n_b \cdot E_b + n_b \cdot R_i \cdot I_{bat} \quad (1)$$

where V_{bat} and I_{bat} are the battery voltage and current (according to the receptor convention), E_b is the electromotive force as a function of the battery state of charge (denoted SOC), and R_i is the internal resistance of an element.

In our application, the battery is composed of 24 electrochemical accumulators in series ("STECO Saphir 3600", product documentation included in the Appendix). According to the manufacturer's characteristics, a single element provides a capacity C_{10} of 325 A.h (with this value representing battery capacity over a discharge regime at constant current during 10 hours: $C_{10} = 10 \cdot I_{10}$) and an internal resistance of 0.4 m Ω .

Three equations are required to describe battery behavior as a function of its charge, overcharge or discharge regime.

The formulation of these equations incorporates the standardized expression of battery capacity C_{bat} , which we shall call "instantaneous capacity" given its dependence upon instantaneous current value and charge history. The state of charge, SOC , of the battery depends on both the residual charge and the actual charge or discharge regime.

III - Capacity model

The capacity model yields the quantity of energy C_{bat} that the battery can restore, according to the average discharge current $\overline{I_{bat}}$. The corresponding expression is established beginning with the I_{10} current, relative to operating mode C_{10} [MAR 03].

$$\frac{C_{bat}}{C_{10}} = \frac{1.67}{1 + 0.67 \cdot \left(\frac{I_{bat}}{I_{10}}\right)^{0.9}} \cdot (1 + 0.005 \cdot \Delta T) \quad (2)$$

where ΔT is the accumulator heating (presumably identical for all elements) in comparison with a 25°C ambient temperature.

C_{bat} is used as a reference to determine battery *SOC*, which will then be formulated according to the quantity of lacking battery charge, Q_d .

$$EDC = 1 - \frac{Q_d}{C_{bat}} \quad (3)$$

IV - Continuous estimation of C_{bat}

The electrical model implies knowledge of the value of instantaneous capacity C_{bat} on a continuous basis. We thus consider that if the battery were fully-charged (i.e. $SOC = SOC_{MAX}$, with the computation imposing an SOC_{MAX} value of 0.9 in order to avoid exceeding the gassing limit (see Section 3.1.3)), this instantaneous capacity C_{bat} would equal the reference value C_{10} . In other cases (i.e. $SOC < SOC_{MAX}$), C_{bat} is calculated on the basis of the equation provided by the CIEMAT model. Accordingly, at any time t , $C_{bat}(t)$ is calculated from the average discharge current, which gets calculated over a period beginning at the instant when the state of charge was maximal until time t , in including only the discharge-specific currents. The following figure illustrates this computation over one operating cycle:

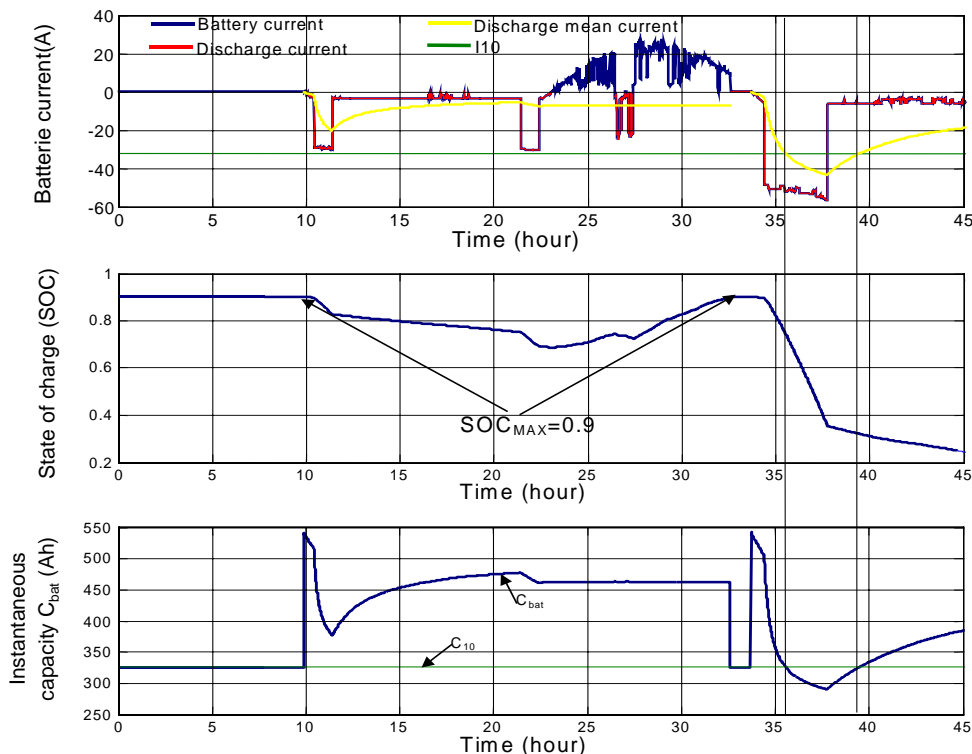


Figure 3: Method for continuously calculating the instantaneous capacity C_{bat} over a given operating cycle (example of battery with capacity $C_{10} = 320$ A.h) - maximum state of charge imposed at 0.9

From this figure, we can observe that if average discharge current falls below I_{10} , then the capacity C_{bat} capable of recharging the battery is greater than C_{10} . Otherwise, if this average current lies above I_{10} , then C_{bat} is less than C_{10} . The instantaneous battery capacity $C_{bat}(t)$ is hence a function not only of the battery's operating mode at time t , but also of how the battery had been used up until t .

V - The voltage equation

The expression for battery voltage has been derived from Equation 2 above as a function of its charge (index "c"), discharge (index "d") or overcharge (index "oc") regime. This set-up thereby leads to a structure tied to both of the battery's internal elements: the electromotive force and the internal resistance [MAR 03]:

$$\left\{ \begin{array}{l} V_{bat_d} = n_b \cdot [1,965 + 0,12 \cdot EDC] - n_b \cdot \frac{|I_{bat}|}{C_{10}} \cdot \left(\frac{4}{1 + |I_{bat}|^{1,3}} + \frac{0,27}{EDC^{1,5}} + 0,02 \right) \cdot (1 - 0,007 \cdot \Delta T) \\ V_{bat_c} = n_b \cdot [2 + 0,16 \cdot EDC] + n_b \cdot \frac{I_{bat}}{C_{10}} \cdot \left(\frac{6}{1 + I_{bat}^{0,86}} + \frac{0,48}{(1 - EDC)^{1,2}} + 0,036 \right) \cdot (1 - 0,025 \cdot \Delta T) \\ V_{bat_oc} = n_b \cdot V_g + n_b \cdot (V_{ec} - V_g) \cdot \left[1 - \exp\left(\frac{t - t_g}{\tau_g}\right) \right] \end{array} \right. \quad (4)$$

During the charge regime, once voltage at the battery terminals has reached V_g (the so-called "gassing voltage"), then the evolution in voltage displays a sharp rise, which characterizes the gaseous release of hydrogen and oxygen: this phenomenon is known as "gassing". The temporal evolution of this phenomenon is approximated by means of an exponential law. The voltage expression can then be established from the point in time t_g , whereby $V_{bat_c} = V_g$ [MAR 03].

The values of gassing voltages V_g and ending charge V_{ec} , along with that of the time constant τ_g , are obtained on the basis of the following expressions [MAR 03]:

$$\left\{ \begin{array}{l} V_{ec} = \left[2,45 + 2,011 \cdot \ln\left(1 + \frac{I_{bat}}{C_{10}}\right) \right] \cdot (1 - 0,002 \cdot \Delta T) \\ V_g = \left[2,24 + 1,97 \cdot \ln\left(1 + \frac{I_{bat}}{C_{10}}\right) \right] \cdot (1 - 0,002 \cdot \Delta T) \\ \tau_g = \frac{1,73}{1 + 852 \cdot \left(\frac{I_{bat}}{C_{10}}\right)^{1,67}} \end{array} \right. \quad (5)$$

VI - Energy efficiency considerations

We will distinguish herein between two types of efficiency: Coulomb and global. The former concerns the capacity of the battery to store energy and excludes Joule losses in the internal resistance, whereas global efficiency includes both Coulomb and Joule losses.

Coulomb efficiency during battery discharge is assumed to equal 100% [DUM 99]:

$$\eta_{cb_d} = 1 \quad (6)$$

Coulomb efficiency during the charge regime depends heavily on the charging rate: its value nears 100% for low charge currents and a weak state of charge; it then deteriorates upon approaching a fully-charged state. The following expression [DUM 99] reveals this relationship:

$$\eta_{cb_c} = 1 - \exp \left[\frac{20.73}{\frac{I_{bat}}{I_{10}} + 0.55} \cdot (SOC - 1) \right] \quad (7)$$

Global efficiency incorporates losses within the internal resistance of the battery to discharge, i.e. when the battery is fully-charged and internal resistance remains low; these losses then increase with a low state of charge, which causes discharge efficiency to considerably decline over this operating zone. While the battery is charging, internal resistance still depends on the state of charge of the electrochemical accumulator. This value rises at an increasing rate when approaching the fully-charged state. From a constant current perspective, the amount of losses will be greater upon approaching the full charge, and efficiency during accumulator charge will thereby be lower over this zone.

For illustration, Figure 4 displays the evolution in internal resistance for our accumulator, which is composed of 24 elements in series during both the discharge and charge regimes:

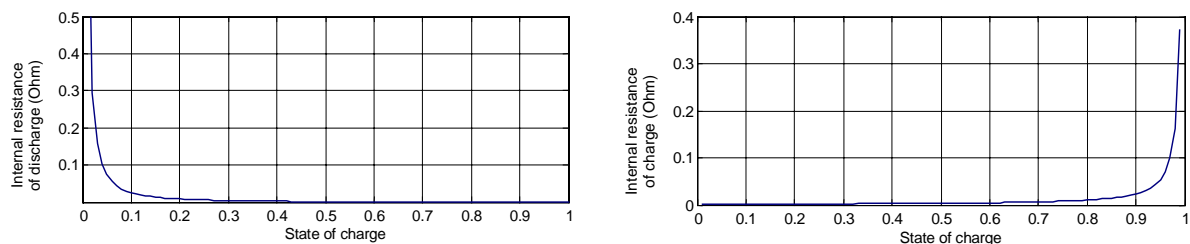


Figure 4: Evolution in the internal resistance of our battery as a function of its state of charge - constant current mode of operations - CIEMAT model conditions

We have computed and then represented in Figure 5 the evolution in global efficiency (Coulomb efficiency + Joule losses) of the battery during both charge and discharge, with respect to its state of charge and the power injected or extracted. For the purpose of this calculation, we imposed constant power during charge and discharge and observed the evolution in state of charge relative to C_{bat} . During charge, efficiency η_{G_c} reflects the ratio of energy stored over this short period to input electrical energy; during discharge, η_{G_d} is the ratio of depleted electrical energy to initially-stored energy.

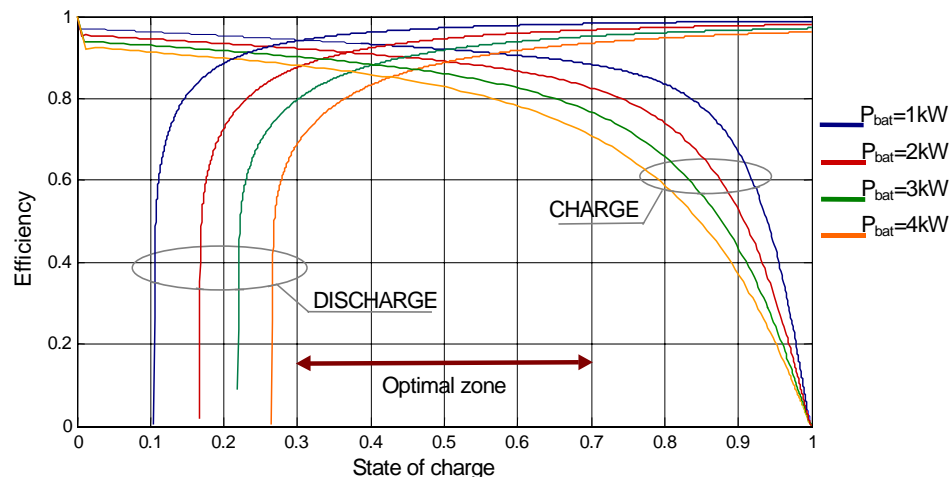


Figure 5: Display of the evolution in global efficiency during both charge and discharge as a function of the state of charge at constant power

During charge, global efficiency becomes even lower as the state of charge nears unity. As recharge power increases, efficiency falls. During discharge, efficiency climbs to almost 100% for a fully-charged battery and tends to zero for weaker states of charge. During discharge, we have

observed that it is impossible to extend below a certain threshold state of charge. As an example, for a 1-kW discharge, we are unable to drop below 10% of the state of charge, whereas at 4 kW this threshold lies at 27%, since the power required is not sufficient to compensate for losses in internal resistance.

We have identified however a preferred operating zone for the battery, roughly between 30% and 70% of the state of charge; over this zone, the battery may be placed into service and delivers acceptable efficiency levels. It can be deduced therefore that an electrochemical battery operating at full power is not functioning over its entire state of charge range. The ensuing loss in potential is considerable and depends on the desired power level, i.e. on the speed of either the charge or discharge.

VII - Simulation on a given cycle

We have tested this model on a battery load-discharge cycle at our experimental facility and have loaded the battery by acting upon the voltage set point imposed by the inverter. Figure 6 displays the stress cycle generated: measured voltage differs slightly from the set point once the current has reached the limits imposed by the inverter. We can note that the set point is not perfectly respected, with the deviation being due to the level of inverter resolution (by means of 0.5-V increments).

According to this simulation, initialization was performed for a measured (and stabilized) uncharged battery voltage of 51.32 V, hence at an 86% state of charge. Figure 7 presents the currents and exchanged energies, which are both measured and computed within an imposed voltage operating range.

We are able to state that while these results appear to be quite close at the beginning of the simulation, they increasingly move apart over time. It can clearly be observed that within an imposed voltage operating range, this model proves to be of limited reliability for the purposes of a systems energy analysis. In this instance, over a span of just beyond 60 hours, total error committed amounts to 1.83 kWh, the equivalent of more than 25%. The act of imposing a voltage set point necessitates knowing with great precision both the electromotive force and internal resistance of the batteries in order to determine the current evolution. The electrical model errors thus induce a cumulative effect on energy estimation, with the current being given in Equation 8 below:

$$I_{bat} = \frac{V_{bat} - n_b \cdot E}{n_b \cdot R_i} \quad (8)$$

Since the order of magnitude of internal resistance is very difficult to determine, an estimation error engenders this same error on the current.

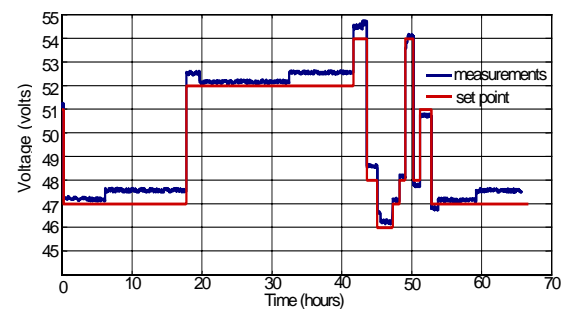


Figure 6: Battery voltage set point and measured voltage over a loading cycle generated via the inverter

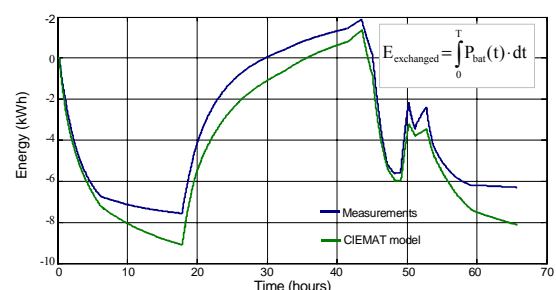
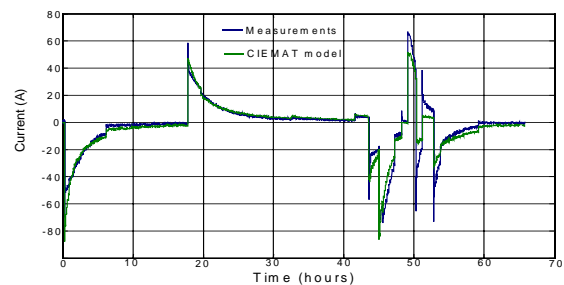


Figure 7: Battery current and exchanged energy vs. time: comparison between measurements and CIEMAT model results - over an imposed voltage operating range

From a practical standpoint with respect to system energy management, it would be advantageous to define a series of power profiles, which gives rise to the notion of imposing a power set point instead of a voltage set point, thereby enabling added evaluation accuracy during both the modeling process and state of charge monitoring. The evolution in current is then calculated from the battery terminal voltage values V_{bat} :

$$\begin{cases} I_{bat} = \frac{P_{bat}}{V_{bat}} \\ V_{bat} = n_b \cdot E + n_b \cdot R_i \cdot I_{bat} \end{cases} \quad (9)$$

Though battery terminal voltage also depends upon internal resistance, the determination of current by means of Equation 9 remains less sensitive to this resistance than in the case of Equation 8. We thus derive the following results for the same operating cycle as above (see Figure 6):

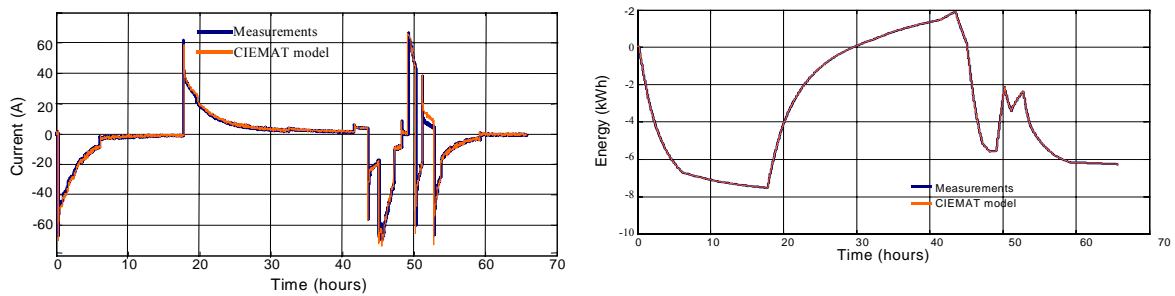


Figure 8: Battery current and exchanged energy: comparison between measurements and CIEMAT model results within an imposed power set point cycle

Figure 8 reveals that by imposing the power value, the CIEMAT model serves to correctly recompose the current within the battery. The battery state of charge may thus be easily obtained by means of coulometry.

We are thereby proposing the following synoptic diagram for calculating both the set points and state of charge:

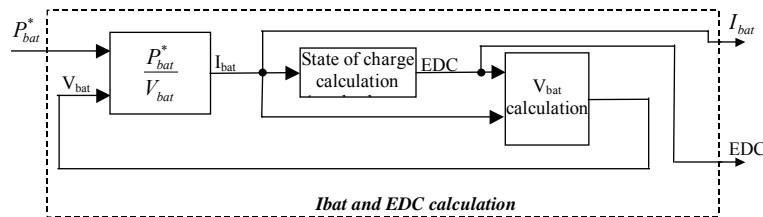


Figure 9: Synoptic diagram for computing the current and state of charge, within an imposed power mode of operations (charge or discharge)

In some cases however, the power set point may not be satisfied:

- the battery state of charge possesses minimum and maximum threshold values. Should the imposed power set point cause the EDC to exceed these thresholds, then: $P_{bat}=0$;
- the current capable of circulating between the continuous bus and the inverter is limited to a maximum absolute value I_{max} . If the power set point engenders a threshold current value, then P_{bat} will be clipped in order to obtain: $|I_{bus}| \leq I_{max}$.

VIII - Energy-based validation of this model over a given operating cycle

We have conducted a comparison between measurement values and model results under actual use conditions. For the simulation of the entire system, we took a reading of the various characteristic magnitudes during normal and autonomous operations, through examining a simplified consumption pattern (daily-period, square wave cycle) connected to the backup network. This consumption pattern features a base consumption of 120 W with peaks at 1,450 W for three hours in cumulative time terms. A default in the primary network, caused after 9½ hours of readings with operations returning to normal 38 hours later, was then simulated. Figure 10 serves to illustrate this simulated situation:

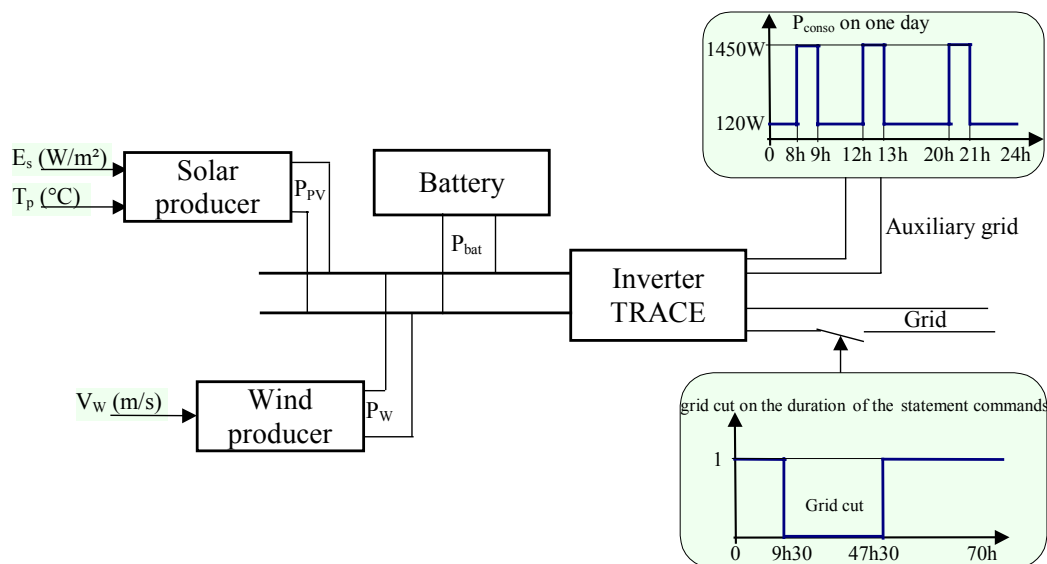


Figure 10: Simulation conditions

Figure 11 presents the results from both measurements and simulation. Attention should initially be drawn to the strong level of qualitative agreement obtained between the two. Despite the presence of certain differences, which are inevitable given the approach employed to accommodate actual reading conditions (power regulation for the simulation, instead of voltage regulation in reality), we were still able to reproduce a highly-realistic energy behavior for such a system and for the given operating cycle.

The table below allows quantitatively comparing the various types of energies involved. As for solar energy, we would like to point out a slight difference (1.6%), which may be attributed to modeling errors [GER 02]; as for wind energy, the difference most likely stems from poor knowledge of the wind actually entering the wind turbine [GER 01].

	Measurement values	Simulation results
Solar energy production	25.1 kWh	25.5 kWh
Wind energy production	0.5 kWh	1.5 kWh
Energy conveyed by the battery	18.1 kWh	19 kWh
Energy consumed by the backup network	19.4 kWh	19.4 kWh
Energy supplied by the primary network	-1.9 kWh	-3 kWh

Table 1: Comparison of the various energies studied

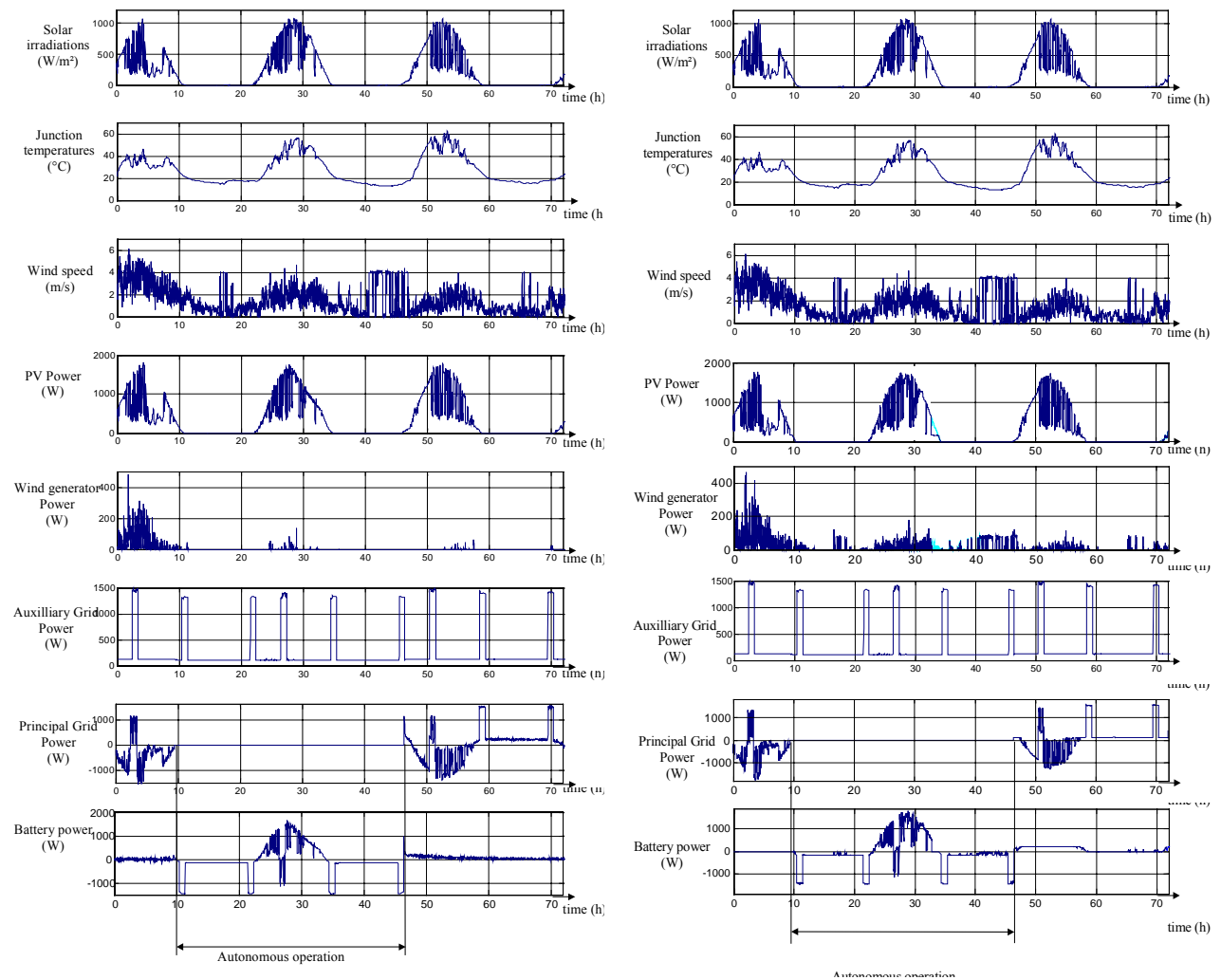


Figure 11: Current system operations with one simplified consumption profile that includes coupling to the network and another operating autonomously
 Left: MEASUREMENT READINGS; Right: SIMULATION RESULTS based on weather data (wind speed, insolation, ambient temperature) and the actual consumption cycle

Figure 12 displays the energy exchanged (both measured and calculated) by the battery and the evolution in its state of charge (simulation). Over the first portion (up to 30 hours), the power supplied or received by the battery is imposed by the production systems and the consumer, with measurement and simulation being performed under the same conditions (imposed powers \cong power set point); we thereby obtain a very high level of agreement between measurement readings and simulated results. In practice over the load-shedding zone, power is no longer imposed by the production systems and a sizable level of disagreement arises between exchanged energy measurements and simulation results. Afterwards, we once again enter into a zone of good agreement until the time network operations have been restored, during which the charge is imposed, in practical terms, by means of a voltage set point as opposed to a power set point for the simulation. The energy conveyed through the battery is equal to the sum of incoming and outgoing energies, which are both counted as positive. The difference in energy received by the network stems from the difference in production systems (and primarily the wind production system). At the beginning of simulation, the state of charge of the accumulator is 90%. When this level of charge is once again reached within the load-shedding zone, the value of energy exchanged by the battery at this very instant thus represents the losses dissipated in this zone since the beginning of the cycle.

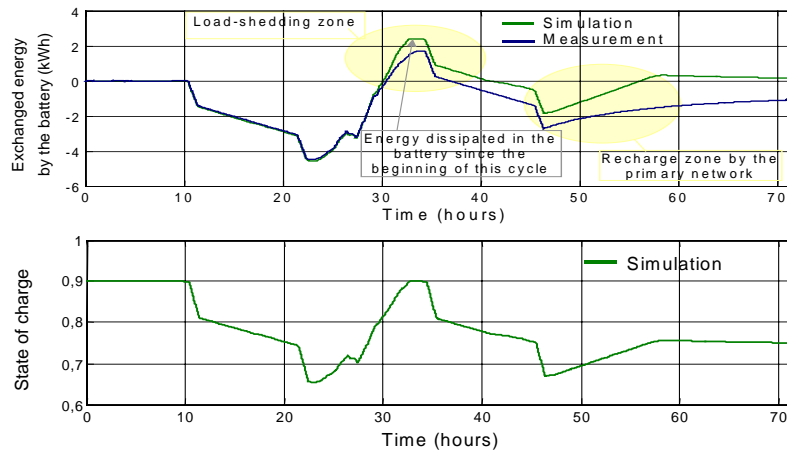


Figure 12: Energies exchanged (measured and calculated) by the battery and evolution in the state of charge (simulated)

IX - Conclusion

This article has focused on the modeling of electrochemical batteries in the aim of deriving a complete energy model of a reduced-power photovoltaic/wind production system coupled to the supply network via a continuous bus with the capacity to operate autonomously.

In light of the complexity involved in modeling the behavior of an electrochemical accumulator, we made use of the CIEMAT model and demonstrated that, provided a regulated-power mode of operations, such a model enabled adequately determining the evolution in battery current; moreover by means of coulometry, we were able to correctly assess its state of charge.

X - References

- [COP 93] J.B. COPETTI, E. LORENZO, F. CHENLO, "A general battery model for PV system simulation", Progress in Photovoltaics: Research and Applications, Vol. 1, pp. 283-292, 1993.
- [DUM 99] C. DUMBS, « Développement d'outils pour l'analyse des systèmes hybrides photovoltaïque-diesel », Ph.D. thesis, Ecole des mines de Paris, defended on December 20, 1999.
- [GER_01] O. GERGAUD, B. MULTON, H. BEN AHMED, « Modélisation d'une chaîne de conversion éolienne de petite puissance », Electrotechnique du Futur 2001, November 2001, Nancy, France, pp. 17-22.
- [GER_02] O. GERGAUD, B. MULTON, H. BEN AHMED, "Analysis and Experimental Validation of various Photovoltaic System Models", 7th International ELECTRIMACS Congress - 2002, August 2002, Montreal, Canada.
- [MAR 03] I. MARIE-JOSEPH, « Méthodologie de diagnostic appliquée à la maintenance préventive d'unités de production d'électricité en sites isolés », Ph.D. thesis, Université des Antilles et de la Guyane, defended on April 07, 2003.
- [GIR_01] F. GIRAUD, Z.M. SALAMEH, « Steady-State Performance of a grid-Connected Rooftop hybrid Wind-Photovoltaic Power System with Battery Storage », IEEE Trans on Energy Conversion, Vol 16, n°1, March 1994, pp. 1-7.